

Color Tuning by Spontaneous Propagation of Gap Surface Plasmons in Epsilon Near Zero Nano-Cavity

Giuseppe Emanuele Lio,^{†,‡} Antonio Ferraro,^{*,†,‡} Michele Giocondo,[‡]
Roberto Caputo,^{*,†,‡,¶} and Antonio De Luca^{†,‡}

[†]*University of Calabria, Physics Department,
87036 Arcavacata di Rende (CS), Italy*

[‡]*CNR-Nanotec, Cosenza 87036 Arcavacata di Rende (CS), Italy*

[¶]*Institute of Fundamental and Frontier Sciences, University of Electronic Science and
Technology of China, Chengdu 610054*

E-mail: antonio.ferraro@unical.it; roberto.caputo@unical.it

Abstract

This work presents numerical and experimental results of plasmonic Metal-Insulator optical nano-cavities. The systems are composed of Silver as metal, polyvinylpyrrolidone or indium tin oxide or zinc oxide as insulator. The proposed nano-cavities exhibit extraordinary effects as colors changing in function of the incident/view angles, enhancement of the experimental real and imaginary parts of the pseudo dielectric constant, an extraordinary transmission of 50% and zero reflection for both polarizations at the resonant wavelengths. These results lead to the formation and propagation of surface plasmon polaritons and their hybridization in gap surface plasmons. The concurrence of these effects allow studying the Goos-Hänchen shift by exploiting the very narrow Δ and Ψ ellipsometer parameters. Thank to their optical properties, the proposed nano-cavities could be applied in several fields such tunable color filters, optics, photonics and sensing.

Keywords

ENZ, Ellipsometry, Optical nano-cavity, Plasmonics, sensing

Introduction

Nanotechnologies based on plasmonic and photonics effects, thanks to the interaction between light and matter at the nanoscale, are involved in several applied field as enhanced Raman spectroscopy, bio-sensing, transistor^[1–6]. Furthermore, the light propagation into nano-guided system could be exploited for the fabrication of subwavelength optics and nano-optical devices^[7–9]. A Polariton is an electromagnetic wave coupled to a polarization excitation in matter^[10–12]. When this coupled excitation occurs at the interface between two media, it is called a surface polariton^[13]. The latter is an evanescent electromagnetic wave that propagates along the interface with amplitude decaying exponentially into the two media. When one of the media is a metal and the other a dielectric, the propagating waves are referred as surface plasmon polaritons (SPPs). Since the discovery of the SPPs, the plasmon resonance at small gaps in metallic subwavelength structures has attracted interest in terms of spectroscopy behavior. An open research field, in particular, is represented by systems composed of Metal/Insulator/Metal (MIM) that are of scientific interest because of the dielectric singularities that appear in the anisotropic permittivity due to ε_{NZ} (NZ stands for near zero) con-

ditions^[14–16]. When the dielectric layer is thicker (hundreds of nanometers) than the metal layers (tens of nanometers), the system behaves as a nano-optical cavity. These systems allow efficient concentration and confinement of electromagnetic energy and can be used for numerous applications as light emission and detection^[17], photovoltaic^[18–20], Bragg reflector^[21,22], plasmonic devices^[23,24], for optics and the related applications^[22,25,26], telecommunications^[24,27], and others^[28–30]. Under a physical point of view, when metal/insulator and insulator/metal interfaces are close to each other, the dispersion curve of the single interface splits into high and low energy modes.^[31] This gives the possibility to excite the surface plasmon by a free space wave without momentum matching simply by perpendicular incidence to the bare metallic end-face of the MIM^[32]. At the interfaces of the MIM, spontaneous surface plasmon polaritons (SPPs) arise whose electric field overlaps within the insulator layer. However, in the MIM system due to the matching of the field symmetry, only the low energy mode is excited (using a p-polarized electromagnetic wave). In case of a MIMI system, it is instead possible to excite both low and high (guided) energy modes, respectively with p- and s-polarized light.^[33–35] In presence of the hybridization of the SPPs excited at the two metal interface and decayed in the thick dielectric layer, it has been numerically and experimentally demonstrated the formation of gap surface plasmons (GSPs) that are related to high energy modes^[31,36–39]. Although several studies of GSPs are reported in literature, the problem of reproducible fabrication of small nanometric gaps persists. In this manuscript, an easy way is proposed to design and fabricate large-area plasmonic cavity resonator in which a dielectric layer of a few hundred nanometers is employed as a gap between the metal layers. The proposed nanocavity has been designed using numerical ellipsometer analysis (NEA), which is able to fit the ellipsometer spectroscopic measurements retrieving optical constant of materials^[40]. In order to fabricate the real nano-cavities, silver (Ag) is exploited as the metal and, for the insulator, three different materials are considered (polyvinylpyrrolidone (PVP), indium tin oxide (ITO) and zinc oxide (ZnO)). The ellipsometric characterization of

the proposed systems reveals very interesting optical features such as extraordinary transmittance^[41] and 0% reflectance for both exciting polarizations (p and s). Furthermore, the ellipsometric parameters Ψ and Δ are measured. These are related to the reflectance ratio $\rho = \tan(\Psi)e^{-i\Delta}$, that includes the amplitude component, calculated as $\Psi = \arctan(r_p/r_s)$ with $r_{p(s)}$ being the $Re\{\sqrt{R_{p(s)}}\}$, and the phase difference evaluated as $\Delta = \phi_p - \phi_s$ ^[40]. In presence of the plasmonic resonance, due to the SPPs and GSPs formation, these parameters show a particular sigmoidal behavior leading to the enhancement of the real and imaginary part of the pseudo dielectric constant. The constant is calculated as $\langle \tilde{\epsilon} \rangle = \langle \epsilon_1 \rangle - i \langle \epsilon_2 \rangle = \sin^2\theta_{inc}[1 - \tan^2\theta_{inc}(\frac{1-\rho}{1+\rho})^2]$ ^[42], where θ_{inc} is the incident angle. Due to the presence of ρ in the previous expression, $\langle \tilde{\epsilon} \rangle$ is directly related to Ψ and Δ . Under specific conditions, $\langle \epsilon_2 \rangle$ can reveal a gain behavior of the system reaching very high absolute values (500) for the MIMI system with ZnO as insulator. Due to their plasmonic behavior, the fabricated nano-cavities present a macroscopic optical effect characterized by different colors when incident light and viewing angles are tuned^[43–47]. Finally, behavior of Δ and Ψ evidence the presence of a spontaneous Goos-Hänchen shift effect^[48–50]. This effect is observed as a small lateral shift between the p and s directions of linearly polarized light undergoing total internal reflection. The counterpart of this effect for circular and elliptical polarization is the Imbert-Fedorov effect^[51]. The Goos-Hänchen effect arises when both waves are reflected from the surface and undergo different phase shifts, that lead to the lateral shift of the probe beam. As demonstrated in previous works^[52,53], the phase shift appears when resonant modes are induced within an optical dielectric cavity, as in the proposed MIMI. In fact, in presence of a multi-layered systems ending with a dielectric layer, as in case of a Bragg reflector or a dielectric mirror, it is possible to evaluate the Goos-Hänchen shift at the resonant wavelength as $\Delta_{s/p}(\theta_{inc}) = 2t_1\tan(\theta_{inc})$. In the previous, t_1 is the thickness of first dielectric layer in the MIMI configuration. The proposed systems, exhibiting this effect, can be involved in a wide scenario of scientific research such as nanopho-

tonics applications^[49], sensitive detection of biological molecules^[54–56], or for the phenomenological study of the lateral reflection for both polarizations^[57].

Results and discussion

Extraordinary transmission in polymeric MIM

In order to fully investigate, both numerically and experimentally, the extraordinary features of the fabricated nano-cavities, see methods for information about the fabrication, we first considered a silver layer with thickness of 40nm deposited on glass substrate. As expected, the transmittance presents a peak only in the UV range at around 330nm with a maximum of the 30%, while the other wavelengths (solid lines with symbol) are reflected. The experimental results agree very well with the numerical one (solid lines)^[40] as reported in Fig. 1a. Then, the Ag thickness has been divided in two parallel layer of 20nm each, placing between them a PVP layer of 380nm . A MIM nano-cavity Ag/PVP/Ag has been created which presents an interesting optical behavior. In fact, in Fig. 1b it is possible to recognize a three main peaks/dips in transmittance/reflectance at specific resonant wavelengths namely in this case at blue, green and red. Moreover, when the MIM is placed at specific small angles it appears transparent - bottom-left of Fig. 1c- while at higher angles it appears colored both in reflection or transmission, as shown in the other sub-pictures of Fig. 1c. This angle sensitive could arise from the plasmonic nature at the resonant wavelength due to the multiple SPPs and GSPs formation at the two metal surfaces and inside the PVP layer, respectively, as explained in the previous paragraph. The ellipsometer parameters Ψ and Δ , reported in the supplementary figure S1, confirm that the fabricated Ag/PVP/Ag MIM is, also, extremely sensible to the polarization (p or s-pol) of the incident wave. These parameters show a giant enhanced Goos-Hänchen shifts^[58]. Even if the fabrication process of the MIM can lead to some inhomogeneities, the agreement between numerical and experimental results is quite satisfactory.

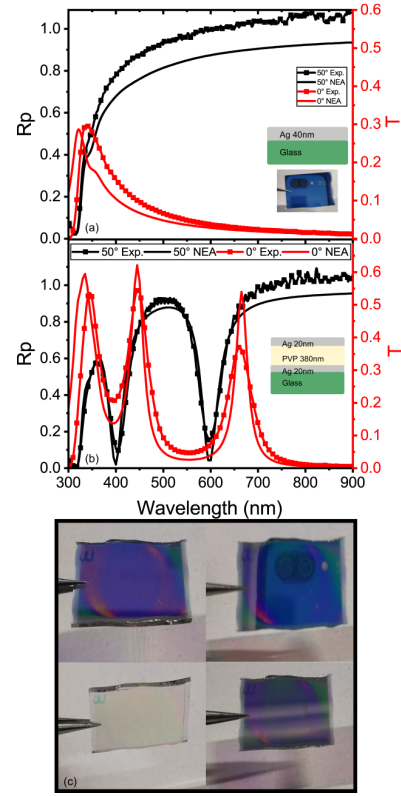


Figure 1: a) Numerical and experimental reflectance (p-pol) at 50° and transmittance at 0° of a silver with thickness of 40nm . The insets report a schematic view of the fabricated system with the thickness of each layer and a real picture where the incident light is completely reflected. b) Numerical and experimental reflectance (p-pol) at 50° and transmittance at 0° of MIM nano cavity composed of Ag/PVP/Ag. The insets report a schematic view of the fabricated system with the thickness of each layer. c) Pictures showing colors dependence on the incident/view angles.

Using polymer as insulator in MIM systems give the opportunity to create very thick insulator layer (hundreds of nanometers), hence many peaks/dips are present in the visible range according to the relation dispersion of a MIM, as shown in Fig 1b. However the PVP layer can be damaged during the second Ag layer sputtering deposition. In order to realize systems more stable than the PVP one, we numerically designed and experimentally fabricated nano-cavities using two solid dielectrics: ITO and ZnO.

ITO MIMI characterization

During the numerical designs and the experimental investigation, it has been observed a substantial difference between a classical MIM and a new MIMI metamaterial configuration. The latter presents an accentuate sigmoidal shape in Ψ and Δ enabling the related study of the plasmonic excitation effects and the Goos-Hänchen shift, while the MIM does not present this feature. The comparison between numerical reflectances for both polarizations, Ψ , and Δ parameters for a MIM and MIMI is shown in Fig. S2. The first realized Ag/ITO/Ag/ITO MIMI is composed of ITO layers of thickness $t_1 = 65nm$ and $t_2 = 20nm$, respectively (see inset of Fig. 2a). The experimental measurements show transmittance of 50% at 0° at the resonant wavelength of $\lambda = 500nm$, see Fig. 2a. On the other hand, the reflectance (p-polarization) at 50° , 60° and 70° is almost zero around the resonant wavelength $\lambda = 480nm$. The MIMI reflectance under s-polarization, reported in Fig.S3a, shows two dips close to the same resonant wavelength of p-pol leading to the particular feature in Ψ and Δ parameters shown in Fig. 2b, c. In fact, Ψ and Δ present a drastic change in their curves with an accentuate sigmoidal shape at $\lambda = 480nm$, enhanced for this particular MIMI at 70° see Fig. 2b,c (blue curve). Hence, the Ψ and Δ parameters highlight the presence of plasmonic excitation for high and low energy modes at the resonant wavelength especially if the system is impinged from an electromagnetic wave with an incident angle of 70° . For the second realized Ag/ITO/Ag/ITO MIMI, the first ITO layer is increased to a thickness $t_1 = 85nm$ (see inset of Fig. 2d) while the thickness of the other layer remains unchanged. The increase of the ITO layer of only $20nm$ leads to the shift of $50nm$ of the resonant wavelengths, where the main transmitted peak is now at $\lambda = 550nm$ with again a value of almost 50%, the reflectance dips (p-polarization) at 50° , 60° and 70° is almost zero around the resonance wavelength $\lambda = 532nm$, see Fig. 2d. The reflectance for s-pol is reported in Fig S4a. The parameters Ψ and Δ for this thicker ITO layer ($t_1 = 85nm$) exhibit the same behavior of the thinner one -see Figs. 2e,f- namely for an incident angle of 70° Δ presents a sigmoidal

shape with an high amplitude. This feature can be exploited in a future applications related to the Goss-Hanchen shift^[55,56]. Hence, it is possible to tune easily the resonant wavelengths without affecting the performance of the system. In order to support the experimental results the reflectances (p and s-pol), transmittance, Ψ and Δ have been numerically evaluated and reported in Fig S2b,c and S3b,c.

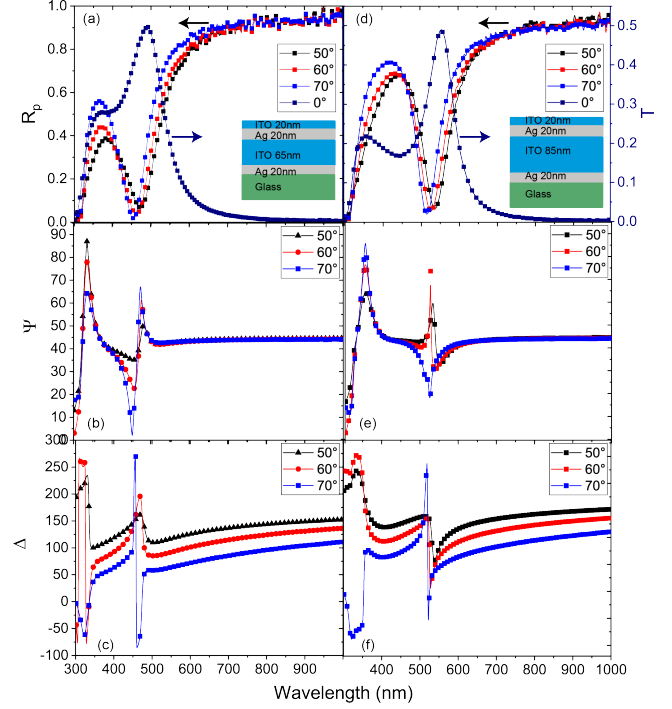


Figure 2: a) Reflectances (p-pol), and transmittance at different incident angles for the MIMI (Ag/ITO/Ag/ITO) made by the ITO layer $t_1 = 65nm$, the inset reports a schematic view of the whole fabricated system with the related thickness of each layer. b,c) Ψ and Δ for that plasmonic nano-cavity. d) Reflectances (p-pol), and transmittance at different incident angles for the MIMI composed of the ITO layer of $t_1 = 85nm$, the inset shows the whole fabricated system with the new layers thickness. d,e) Ψ and Δ for the second MIMI.

A further investigation has been done using COMSOL Multiphysics, indeed, it has been studied how the electromagnetic field (\mathbf{E}) interacts with the entire system producing the coupled plasmons. Fig 3 shows the \mathbf{E} , at resonance ($\lambda = 480nm$) and out of resonance ($\lambda = 700nm$), for

the MIMI realized with the ITO layer of $65nm$. In particular, it is possible to observe that most part of the \mathbf{E} is confined in the nano-cavity dielectric layer exciting a single (high or low energy) mode while the remaining part of \mathbf{E} passes through the system, see Fig 3a, b. It has been highlighted that for p-pol the main low energy mode is generated from the SPPs hybridization that decays inside the dielectric cavity, while the s-pol wave excites high energy mode (GSP). Instead, out of the resonance condition the electromagnetic field is totally reflected with no interaction with the thicker ITO layer, see Fig 3c, d. The electric field maps related to the second fabricated MIMI (ITO $t_1 = 85nm$) are illustrated in the supplementary information in figure S5.

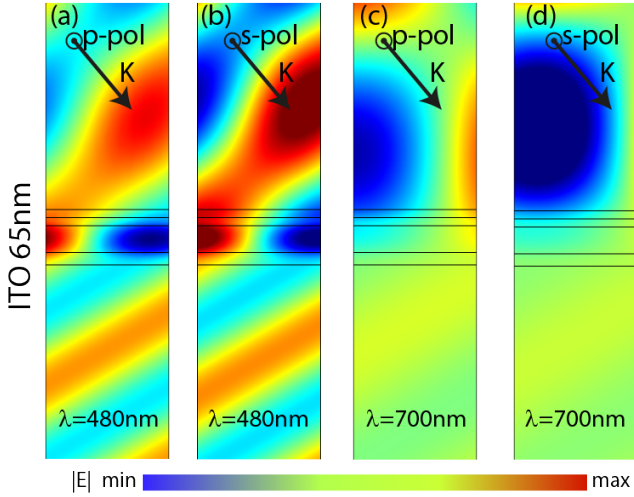


Figure 3: Electric field maps for the MIMI composed of Ag/ITO/Ag/ITO with thicknesses of 20/65/20/20nm respectively. a , b) at the resonant wavelength of $\lambda = 480nm$ for p and s-polarization where the resonant mode inside the ITO nano-cavity is shown. c, d) Out of resonance at $\lambda = 700nm$ for both polarizations.

The described plasmonic coupling between the incident wave and the system is the main feature of the proposed nano-cavities. In order to investigate how this effect is strongly related to different color changing as function of the incident/view angles, experimental measurements of the real and imaginary part of the pseudo dielectric constants has been done. These quantities are identified in the following as $\langle \epsilon_1 \rangle$ and $\langle \epsilon_2 \rangle$. Fig 4a,b show the pictures of the two MIMI with the ITO

$t_1 = 65nm$ and $t_1 = 85nm$, respectively. The first one shows different colors when it is observed at different angles, how it is shown in bottom and upper-right pictures of Fig. 4a. Instead, at small angles the system permits to see through it a blue color while the reflected light appears gold, see upper-left picture of Fig. 4a. Then, we focused our attention on $\langle \epsilon_2 \rangle$ for understanding the gain and loss optical behavior, related to the GSP and SPP formation, respectively. The experimental results present an high and low energy mode excited at the resonant wavelength ($\lambda = 480nm$) for incident angle of 70° , while excited modes (the value is less than the first ones) for each measured incident angles is observed at $\lambda = 327nm$ representing the Ferrel-Berreman mode of Silver^[59], see Fig4b. The second MIMI present different colors passing from the green to the purple due to the increased thickness as illustrated in bottom and upper-right pictures of Fig. 4c. At small angles, now, the system allows seeing through it with a green color while the reflected light appears purple, see upper-left picture of Fig. 4c. The experimental $\langle \epsilon_2 \rangle$, reported in Fig. 4d, confirm this optical behavior due to the presence again of an high and low energy mode around the resonant wavelength ($\lambda = 532nm$) for incident angle of 70° , while a moderate second excited mode is observed at $\lambda = 380nm$ for each measured incident angles. Moreover, the Ferrel-Berreman mode is still present. Therefore, these measurements could be used to recognize in a fast and effective way the excitation of a GSP as a gain and of the SPP as a loss in $\langle \epsilon_2 \rangle$. In fact, the $\langle \epsilon_2 \rangle$ measurements are largely used to explain the presence of gain or loss effects in plasmonic materials^[60–66]. In the present case, this has been used to trace the gain/loss condition of the MIMI (related to the high/low modes) in presence of a s- or p-polarized excitation respectively.

ZnO MIMI characterization

Successively, in order to enhance the performance of the plasmonic MIMI nano-cavities, the ZnO has been used as dielectric instead of ITO. Moreover, ZnO in nano-science is largely used thanks to its excellent features in photovoltaics^[67,68], extreme non linearity application as second har-

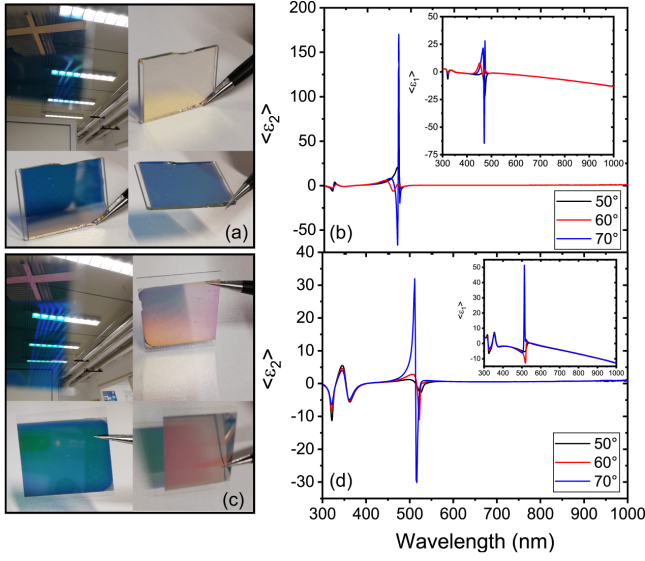


Figure 4: a) The pictures are referred to the MIMI nano-cavity with the ITO thickness equal to $65nm$. The color of the MIMI passes from blue to gold when observed in transmission or in reflection, respectively. b) The graph reports the $\langle \epsilon_2 \rangle$ at three different incident angles while the inset depicts the $\langle \epsilon_1 \rangle$. c) The pictures are referred to the second fabricated MIMI (ITO $t_1 = 85nm$). The nano-cavity color passes from green to purple when it is observed in transmission or in reflection, respectively. d) The graph shows the $\langle \epsilon_2 \rangle$ at three different incident angles, while the inset shows the $\langle \epsilon_1 \rangle$ behavior.

monic generation^[69,70], photocatalysis^[71,72], just to name a few. The nano-cavity is composed of Ag/ZnO/Ag/ZnO and the dielectric layers have the following thickness $t_1 = 83nm$ and $t_2 = 20nm$, see the inset in Fig. 5. The proposed MIMI presents the same optical properties of the previous one: experimentally measured transmittance reaching the 55% at the resonant $\lambda = 530nm$, and 0% reflectance at around ($\lambda = 520nm$), see Fig. 5a. As for the systems with ITO, the GSP and SPP arise inside the ZnO MIMI with the s-polarized reflectance (R_s) presenting a dip close to 0% at the resonant wavelength ($\lambda = 530nm$), see Fig. S6a. These features (R_p and $R_s = 0\%$) allow measuring a very sharp Ψ and Δ , as illustrated in Figs. 5b, c; paving the way to exploit the enhanced Goos-Hänchen shift for sensing applications. This nano-cavity MIMI, due to the accentuate behavior

of Ψ and Δ at each incident angle, presents a remarkable angle color change passing from green color to some shades of purple. In comparison to the ITO MIMIs, the resonance of this system allows transmitting the green component of the light, while the other produce a purple reflection, as it is visible in the pictures of Fig. 5d. This ZnO system works better as filtering component at the resonant wavelength due to the less influence of the Ferrel-Berremann mode. The measured enhanced pseudo $\langle \epsilon_2 \rangle = |500|$ at $\lambda = 530nm$ for the incident angle 50° correspond to main excited cavity modes (the high and low energy), see Fig. 5e. Moreover, at the other incident angles (60° , 70°) gain resonant mode are still present confirmed by the measured sigmoidal shape of Δ parameter. The color change as a function of the incident/view angles is video recorded and available in the supplementary information. All the measured optical properties agree very well with the numerical simulations, which are reported in Figs. S6b,c. The electric field maps at and out of resonance wavelength for that ZnO MIMI has been numerically illustrated in Fig. S7.

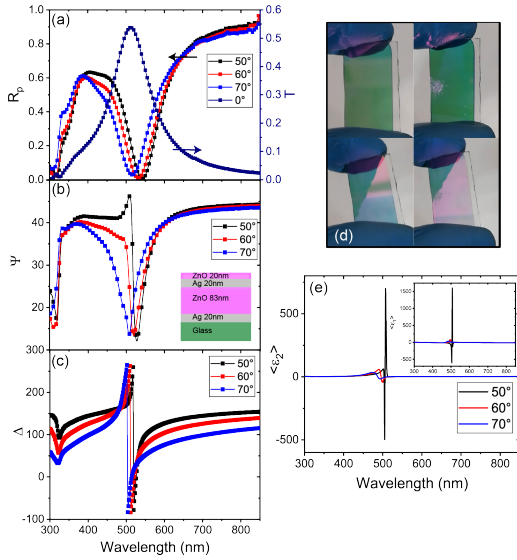


Figure 5: a) Reflectances (p-pol), and transmittance at different incident angles for the MIMI composed of Ag/ZnO/Ag/ZnO with the ZnO layer of $t_1 = 83nm$ and $t_2 = 20nm$, respectively. b,c) Ψ and Δ curves for the fabricated nano-cavity, the inset reports a schematic view of the MIMI with the related thickness of each layer. d) Pictures referred to Ag/ZnO/Ag/ZnO system taken at different incident/view angles. e) $\langle \epsilon_2 \rangle$ at three different incident angles, while the inset shows the $\langle \epsilon_1 \rangle$ curve.

The proposed systems allow realizing sub-wavelength plasmonic cavities without the use of complicate or nano-momentum matching structures. They can be exploited for future applications as sensors, especially considering the giant enhanced Goos-Hänchen shift and its effects^[56,73,74], photovoltaics layers, plasmonic color filter for CMOS sensors^[75], plasmonic for multiple uses^[76], active nano-optics^[77–81]. They can also be exploited for the future physical security systems, for example it is possible to use the Ψ or Δ optical response (or the pseudo dielectric constants due to the sharp curves) as a fingerprint for unclonable and anti-counterfeiting applications.^[82–84]

Conclusions

In this experimental and numerical work, we have presented a comprehensive study of different op-

tical metal/insulator nano-cavities. The systems show particular optical features such as zero reflectances, extraordinary transmittance, sigmoidal behavior of the parameters Ψ and Δ , and the giant enhanced real and imaginary part of the pseudo dielectric constants $\langle \epsilon_1 \rangle$ and $\langle \epsilon_2 \rangle$ at the resonant wavelengths. The MIMI configuration due to the double interface metal-insulator the dispersion curve exhibit high and low-energy modes which can be excited in free space without momentum matching. Hence, all the optical properties possesses by the proposed MIMI nano-cavities systems allow using them as sensors due to the giant enhanced Goos-Hänchen shift. Furthermore, the color changing behavior could be exploited for filtering, physical security systems, and photonics.

Materials and Methods

Samples fabrication Fabrication began depositing silver on glass by using DC sputtering (power 30W and argon pressure of $4.5 \times 10^{-2} mbar$), see the inset of Fig. 1a. Then, for the Ag/PVP/Ag nano-cavities, on the first Ag layer of 20nm the PVP 5% wt. in ethanol is deposited by spin-coating (3000 rpm) resulting in a layer of 380nm measured by atomic force microscopy. Finally, the fabrication of the system is completed depositing silver (20nm) on top of PVP. A schematic view is reported in the inset of Fig. 1b. For the MIMIs composed of Ag/ITO/Ag/ITO the PVP is replaced with a thin layer of ITO deposited by DC sputtering (power 40W and argon pressure of $4.5 \times 10^{-2} mbar$). The thickness of each layer of nano-cavity systems is reported in the inset of Fig. 2. The last MIMI is realized with ZnO instead of ITO.

Characterization The fabricated systems is characterized using a Wase-M2000 Woolam Ellipsometer from 300nm to 900nm with a resolution of 1.5nm in both p and s-polarization with incident angles: 50°, 60°, 70°. The experimental data is plotted with a skip point of 7. The measurements are fitted with a property software. In order to extracted optical constants of the used materials and systems, for each deposition, a reference sample is fabricated and analyzed (single layer of each material).

Numerical simulations The simulations are performed using Numerical Ellipsometer Analysis (NEA) implemented in commercial software COMSOL Multiphysics, see ref [39] for details.

Acknowledgement The authors thank the “Area della Ricerca di Roma 2”, Tor Vergata, for the access to the ICT Services (ARToV-CNR) for the use of the COMSOL Multiphysics Platform, Origin Lab and Matlab, and the Infrastructure “BeyondNano” (PONa3-00362) of CNR-Nanotec for the access to research instruments.

References

1. Xu, H.; Bjerneld, E. J.; Käll, M.; Börjesson, L. Spectroscopy of single hemoglobin molecules by surface enhanced Raman scattering. *Phys. Rev. Lett.* **1999**, *83*, 4357.
2. Chang, D. E.; Sørensen, A. S.; Demler, E. A.; Lukin, M. D. A single-photon transistor using nanoscale surface plasmons. *Nat. Phys.* **2007**, *3*, 807–812.
3. Ward, D. R.; Grady, N. K.; Levin, C. S.; Halas, N. J.; Wu, Y.; Nordlander, P.; Natelson, D. Electromigrated nanoscale gaps for surface-enhanced Raman spectroscopy. *Nano Lett.* **2007**, *7*, 1396–1400.
4. Li, W.-D.; Ding, F.; Hu, J.; Chou, S. Y. Three-dimensional cavity nanoantenna coupled plasmonic nanodots for ultrahigh and uniform surface-enhanced Raman scattering over large area. *Opt. Express* **2011**, *19*, 3925–3936.
5. De Leon, N. P.; Shields, B. J.; Chun, L. Y.; Englund, D. E.; Akimov, A. V.; Lukin, M. D.; Park, H. Tailoring light-matter interaction with a nanoscale plasmon resonator. *Phys. Rev. Lett.* **2012**, *108*, 226803.
6. Berweger, S.; Atkin, J. M.; Olmon, R. L.; Raschke, M. B. Light on the Tip of a Needle: Plasmonic Nanofocusing for Spectroscopy on the Nanoscale. *The Journal of Physical Chemistry Letters* **2012**, *3*, 945–952.
7. Barnes, W. L.; Dereux, A.; Ebbesen, T. W. Surface plasmon subwavelength optics. *Nature* **2003**, *424*, 824–830.
8. De Sio, L.; Caligiuri, V.; Umeton, C. Tuneable broadband optical filter based on soft-composite materials. *J. Opt.* **2014**, *16*, 065703.
9. Lio, G. E.; Madrigal, J. B.; Xu, X.; Peng, Y.; Pierini, S.; Couteau, C.; Jradi, S.; Bachelot, R.; Caputo, R.; Blaize, S. Integration of nanoemitters onto photonic structures by guided evanescent-wave nanophotopolymerization. *The Journal of Physical Chemistry C* **2019**, *123*, 14669–14676.
10. Ruppin, R.; Englman, R. Optical phonons of small crystals. *Rep. Prog. Phys.* **1970**, *33*, 149.
11. Mills, D.; Burstein, E. Polaritons: the electromagnetic modes of media. *Rep. Prog. Phys.* **1974**, *37*, 817.
12. Halevi, P. Polariton modes at the interface between two conducting or dielectric media. *Surf. Sci.* **1978**, *76*, 64–90.
13. Zayats, A. V.; Smolyaninov, I. I.; Maradudin, A. A. Nano-optics of surface plasmon polaritons. *Phys. Rep.* **2005**, *408*, 131–314.
14. Maas, R.; Parsons, J.; Engheta, N.; Polman, A. Experimental realization of an epsilon-near-zero metamaterial at visible wavelengths. *Nat. Photonics* **2013**, *7*, 907.
15. Caligiuri, V.; De Luca, A. Metal-semiconductor-oxide extreme hyperbolic metamaterials for selectable canalization wavelength. *J. Phys. D: Appl. Phys.* **2016**, *49*, 08LT01.
16. Caligiuri, V.; Dhama, R.; Sreekanth, K.; Strangi, G.; De Luca, A. Dielectric singularity in hyperbolic metamaterials: the inversion point of coexisting anisotropies. *Sci. Rep.* **2016**, *6*, 20002.
17. Vahala, K. J. Optical microcavities. *Nature* **2003**, *424*, 839–846.

18. Grover, S.; Moddel, G. Applicability of metal/insulator/metal (MIM) diodes to solar rectennas. *IEEE J. Photovolt.* **2011**, *1*, 78–83.
19. Guo, C. F.; Sun, T.; Cao, F.; Liu, Q.; Ren, Z. Metallic nanostructures for light trapping in energy-harvesting devices. *Light: Science & Applications* **2014**, *3*, e161.
20. Grover, S.; Moddel, G. Engineering the current–voltage characteristics of metal–insulator–metal diodes using double-insulator tunnel barriers. *Solid-State Electron.* **2012**, *67*, 94–99.
21. Hosseini, A.; Massoud, Y. A low-loss metal-insulator-metal plasmonic bragg reflector. *Opt. Express* **2006**, *14*, 11318–11323.
22. Zhang, Q.; Huang, X.-G.; Lin, X.-S.; Tao, J.; Jin, X.-P. A subwavelength coupler-type MIM optical filter. *Opt. Express* **2009**, *17*, 7549–7554.
23. Han, Z.; Forsberg, E.; He, S. Surface plasmon Bragg gratings formed in metal-insulator-metal waveguides. *IEEE Photon. Technol. Lett.* **2007**, *19*, 91–93.
24. Wang, G.; Lu, H.; Liu, X.; Mao, D.; Duan, L. Tunable multi-channel wavelength demultiplexer based on MIM plasmonic nanodisk resonators at telecommunication regime. *Opt. Express* **2011**, *19*, 3513–3518.
25. Hill, M. T.; Marell, M.; Leong, E. S.; Smalbrugge, B.; Zhu, Y.; Sun, M.; Van Veldhoven, P. J.; Geluk, E. J.; Karouta, F.; Oei, Y.-S., *et al.* Lasing in metal-insulator-metal sub-wavelength plasmonic waveguides. *Opt. Express* **2009**, *17*, 11107–11112.
26. Choo, H.; Kim, M.-K.; Staffaroni, M.; Seok, T. J.; Bokor, J.; Cabrini, S.; Schuck, P. J.; Wu, M. C.; Yablonovitch, E. Nanofocusing in a metal–insulator–metal gap plasmon waveguide with a three-dimensional linear taper. *Nat. Photonics* **2012**, *6*, 838.
27. Kim, H.-T.; Park, J.-H.; Kim, Y.-K.; Kwon, Y. V-band low-loss and low-voltage distributed MEMS digital phase shifter using metal-air-metal capacitors. 2002 IEEE MTT-S International Microwave Symposium Digest (Cat. No. 02CH37278). 2002; pp 341–344.
28. Thissen, P.; Schindler, B.; Diesing, D.; Hasselbrink, E. Optical response of metal–insulator–metal heterostructures and their application for the detection of chemi-currents. *New J. Phys.* **2010**, *12*, 113014.
29. Banerjee, P.; Perez, I.; Henn-Lecordier, L.; Lee, S. B.; Rubloff, G. W. Nanotubular metal–insulator–metal capacitor arrays for energy storage. *Nat. Nanotechnol.* **2009**, *4*, 292.
30. Caligiuri, V.; Palei, M.; Imran, M.; Manna, L.; Krahne, R. Planar Double-Epsilon-Near-Zero Cavities for Spontaneous Emission and Purcell Effect Enhancement. *ACS Photonics* **2018**, 2287–2294.
31. Miyazaki, H. T.; Kurokawa, Y. Squeezing visible light waves into a 3-nm-thick and 55-nm-long plasmon cavity. *Phys. Rev. Lett.* **2006**, *96*, 097401.
32. Stegeman, G.; Wallis, R.; Maradudin, A. Excitation of surface polaritons by end-fire coupling. *Opt. Lett.* **1983**, *8*, 386–388.
33. Zia, R.; Selker, M. D.; Catrysse, P. B.; Brongersma, M. L. Geometries and materials for subwavelength surface plasmon modes. *JOSA A* **2004**, *21*, 2442–2446.
34. Dereshgi, S. A.; Okay, A. K. Large area compatible broadband superabsorber surfaces in the VIS-NIR spectrum utilizing metal-insulator-metal stack and plasmonic nanoparticles. *Opt. Express* **2016**, *24*, 17644–17653.
35. Sharma, P.; Dinesh, K. V. Surface plasmon Bragg grating using hybrid metal insulator metal plasmonic waveguide. 2017 Progress in Electromagnetics Research Symposium-Fall (PIERS-FALL). 2017; pp 2747–2751.
36. Miyazaki, H. T.; Kurokawa, Y. Controlled plasmon resonance in closed metal/insulator/metal nanocavities. *Appl. Phys. Lett.* **2006**, *89*, 211126.

37. Kuttge, M.; Cai, W.; de Abajo, F. J. G.; Polman, A. Dispersion of metal-insulator-metal plasmon polaritons probed by cathodoluminescence imaging spectroscopy. *Phys. Rev. B* **2009**, *80*, 033409.
38. Neutens, P.; Van Dorpe, P.; De Vlainck, I.; Lagae, L.; Borghs, G. Electrical detection of confined gap plasmons in metal-insulator-metal waveguides. *Nat. Photonics* **2009**, *3*, 283.
39. Todisco, F.; Esposito, M.; Panaro, S.; De Giorgi, M.; Dominici, L.; Ballarini, D.; Fernández-Domínguez, A. I.; Tasco, V.; Cuscuna, M.; Passaseo, A., *et al.* Toward cavity quantum electrodynamics with hybrid photon gap-plasmon states. *ACS Nano* **2016**, *10*, 11360–11368.
40. Lio, G. E.; Palermo, G.; Caputo, R.; De Luca, A. A comprehensive optical analysis of nanoscale structures: from thin films to asymmetric nanocavities. *RSC Adv.* **2019**, *9*, 21429–21437.
41. Han, Z.; Bozhevolnyi, S. I. Plasmon-induced transparency with detuned ultracompact Fabry-Perot resonators in integrated plasmonic devices. *Opt. Express* **2011**, *19*, 3251–3257.
42. Azzam, R. M.; Bashara, N. M.; Ballard, S. S. Ellipsometry and polarized light. *Physics Today* **1978**, *31*, 72.
43. Xu, T.; Shi, H.; Wu, Y.-K.; Kaplan, A. F.; Ok, J. G.; Guo, L. J. Structural colors: from plasmonic to carbon nanostructures. *Small* **2011**, *7*, 3128–3136.
44. Chen, J.; Yang, J.; Chen, Z.; Fang, Y.-J.; Zhan, P.; Wang, Z.-L. Plasmonic reflectors and high-Q nano-cavities based on coupled metal-insulator-metal waveguides. *AIP Adv.* **2012**, *2*, 012145.
45. Gu, Y.; Zhang, L.; Yang, J. K.; Yeo, S. P.; Qiu, C.-W. Color generation via subwavelength plasmonic nanostructures. *Nanoscale* **2015**, *7*, 6409–6419.
46. Segal, E.; Weissman, A.; Gachet, D.; Salomon, A. Hybridization between nanocavities for a polarimetric color sorter at the sub-micron scale. *Nanoscale* **2016**, *8*, 15296–15302.
47. Caligiuri, V.; Biffi, G.; Palei, M.; Martín-García, B.; Pothuraju, R. D.; Bretonnière, Y.; Krahne, R. Angle and Polarization Selective Spontaneous Emission in Dye-Doped Metal/Insulator/Metal Nanocavities. *Adv. Opt. Mater.* **2020**, *8*, 1901215.
48. Snyder, A. W.; Love, J. D. Goos-Hänchen shift. *Appl. Opt.* **1976**, *15*, 236–238.
49. Wild, W. J.; Giles, C. L. Goos-Hänchen shifts from absorbing media. *Phys. Rev. A* **1982**, *25*, 2099.
50. Lai, H.; Cheng, F.; Tang, W. Goos-Hänchen effect around and off the critical angle. *JOSA A* **1986**, *3*, 550–557.
51. De Fornel, F. *Evanescent waves: from Newtonian optics to atomic optics*; Springer Science & Business Media, 2001; Vol. 73.
52. Foster, D. H.; Nöckel, J. U. Methods for 3-D vector microcavity problems involving a planar dielectric mirror. *Optics communications* **2004**, *234*, 351–383.
53. Foster, D. H.; Cook, A. K.; Nöckel, J. U. Goos-Hänchen induced vector eigenmodes in a dome cavity. *Optics letters* **2007**, *32*, 1764–1766.
54. Jiang, L.; Zeng, S.; Xu, Z.; Ouyang, Q.; Zhang, D.-H.; Chong, P. H. J.; Coquet, P.; He, S.; Yong, K.-T. Multifunctional hyperbolic nanogroove metasurface for submolecular detection. *Small* **2017**, *13*, 1700600.
55. Sreekanth, K. V.; Zeng, S.; Yong, K.-T.; Yu, T. Sensitivity enhanced biosensor using graphene-based one-dimensional photonic crystal. *Sens. Actuators, B* **2013**, *182*, 424–428.

56. Sreekanth, K. V.; Ouyang, Q.; Sreejith, S.; Zeng, S.; Lishu, W.; Ilker, E.; Dong, W.; Elkabbash, M.; Ting, Y.; Lim, C. T., *et al.* Phase-Change-Material-Based Low-Loss Visible-Frequency Hyperbolic Metamaterials for Ultrasensitive Label-Free Biosensing. *Adv. Opt. Mater.* **2019**, 1900081.
57. Merano, M.; Aiello, A.; 't Hooft, G.; van Exter, M. P.; Eliel, E. R.; Woerdman, J. P. Observation of Goos-Hänchen shifts in metallic reflection. *Opt. Express* **2007**, *15*, 15928–15934.
58. Sreekanth, K. V.; Ouyang, Q.; Han, S.; Yong, K.-T.; Singh, R. Giant enhancement in Goos-Hänchen shift at the singular phase of a nanophotonic cavity. *Appl. Phys. Lett.* **2018**, *112*, 161109.
59. Newman, W. D.; Cortes, C. L.; Atkinson, J.; Pramanik, S.; DeCorby, R. G.; Jacob, Z. Ferrell-Berreman modes in plasmonic epsilon-near-zero media. *ACS Photonics* **2014**, *2*, 2–7.
60. de Ceglia, D.; Campione, S.; Vincenti, M. A.; Capolino, F.; Scalora, M. Low-damping epsilon-near-zero slabs: Nonlinear and nonlocal optical properties. *Phys. Rev. B* **2013**, *87*, 155140.
61. Khurgin, J. B.; Boltasseva, A. Reflecting upon the losses in plasmonics and metamaterials. *MRS Bull.* **2012**, *37*, 768–779.
62. Sukhorukov, A. A.; Solntsev, A. S.; Kruk, S. S.; Neshev, D. N.; Kivshar, Y. S. Nonlinear coupled-mode theory for periodic plasmonic waveguides and metamaterials with loss and gain. *Opt. Lett.* **2014**, *39*, 462–465.
63. Johns, P.; Yu, K.; Devadas, M. S.; Hartland, G. V. Role of resonances in the transmission of surface plasmon polaritons between nanostructures. *ACS Nano* **2016**, *10*, 3375–3381.
64. Koenderink, A. F. Plasmon nanocavity array lasers: Cooperating over losses and competing for gain. *ACS Nano* **2019**, *13*, 7377–7382.
65. Song, B.; Yao, Y.; Groenewald, R. E.; Wang, Y.; Liu, H.; Wang, Y.; Li, Y.; Liu, F.; Cronin, S. B.; Schwartzberg, A. M., *et al.* Probing gap plasmons down to subnanometer scales using collapsible nanofingers. *ACS Nano* **2017**, *11*, 5836–5843.
66. Caligiuri, V.; Pezzi, L.; Veltri, A.; De Luca, A. Resonant gain singularities in 1D and 3D metal/dielectric multilayered nanostructures. *ACS Nano* **2017**, *11*, 1012–1025.
67. Lee, Y.-J.; Ruby, D. S.; Peters, D. W.; McKenzie, B. B.; Hsu, J. W. ZnO nanostructures as efficient antireflection layers in solar cells. *Nano Lett.* **2008**, *8*, 1501–1505.
68. Manor, A.; Katz, E. A.; Tromholt, T.; Krebs, F. C. Electrical and Photo-Induced Degradation of ZnO Layers in Organic Photovoltaics. *Adv. Energy Mater.* **2011**, *1*, 836–843.
69. Tritschler, T.; Mücke, O.; Wegener, M.; Morgner, U.; Kärtner, F. Evidence for third-harmonic generation in disguise of second-harmonic generation in extreme nonlinear optics. *Phys. Rev. Lett.* **2003**, *90*, 217404.
70. Neumann, U.; Grunwald, R.; Griebner, U.; Steinmeyer, G.; Schmidbauer, M.; Seiber, W. Second-harmonic performance of a-axis-oriented ZnO nanolayers on sapphire substrates. *Appl. Phys. Lett.* **2005**, *87*, 171108.
71. Yayapao, O.; Thongtem, T.; Phuruangrat, A.; Thongtem, S. Ultrasonic-assisted synthesis of Nd-doped ZnO for photocatalysis. *Mater. Lett.* **2013**, *90*, 83–86.
72. Jaramillo, T. F.; Baeck, S.-H.; Kleiman-Shwarsctein, A.; McFarland, E. W. Combinatorial electrochemical synthesis and screening of mesoporous ZnO for photocatalysis. *Macromol. Rapid Commun.* **2004**, *25*, 297–301.
73. Hashimoto, T.; Yoshino, T. Optical heterodyne sensor using the Goos-Hänchen shift. *Opt. Lett.* **1989**, *14*, 913–915.

74. Yin, X.; Hesselink, L. Goos-Hänchen shift surface plasmon resonance sensor. *Appl. Phys. Lett.* **2006**, *89*, 261108.
75. Yokogawa, S.; Burgos, S. P.; Atwater, H. A. Plasmonic color filters for CMOS image sensor applications. *Nano Lett.* **2012**, *12*, 4349–4354.
76. Roberts, A. S.; Pors, A.; Albrektsen, O.; Bozhevolnyi, S. I. Subwavelength plasmonic color printing protected for ambient use. *Nano Lett.* **2014**, *14*, 783–787.
77. Maier, S. A. Gain-assisted propagation of electromagnetic energy in subwavelength surface plasmon polariton gap waveguides. *Opt. Commun.* **2006**, *258*, 295–299.
78. Lal, S.; Link, S.; Halas, N. J. Nano-optics from sensing to waveguiding. *Nat. Photonics* **2007**, *1*, 641.
79. Karalis, A.; Joannopoulos, J.; Soljačić, M. Plasmonic-dielectric systems for high-order dispersionless slow or stopped subwavelength light. *Phys. Rev. Lett.* **2009**, *103*, 043906.
80. Martín-Cano, D.; Martín-Moreno, L.; García-Vidal, F. J.; Moreno, E. Resonance energy transfer and superradiance mediated by plasmonic nanowaveguides. *Nano Lett.* **2010**, *10*, 3129–3134.
81. Ellenbogen, T.; Seo, K.; Crozier, K. B. Chromatic plasmonic polarizers for active visible color filtering and polarimetry. *Nano Lett.* **2012**, *12*, 1026–1031.
82. Cui, Y.; Hegde, R. S.; Phang, I. Y.; Lee, H. K.; Ling, X. Y. Encoding molecular information in plasmonic nanostructures for anti-counterfeiting applications. *Nanoscale* **2014**, *6*, 282–288.
83. Zheng, Y.; Jiang, C.; Ng, S. H.; Lu, Y.; Han, F.; Bach, U.; Gooding, J. J. Unclonable Plasmonic Security Labels Achieved by Shadow-Mask-Lithography-Assisted Self-Assembly. *Adv. Mater.* **2016**, *28*, 2330–2336.
84. Smith, A. F.; Patton, P.; Skrabalak, S. E. Plasmonic Nanoparticles as a Physically Unclonable Function for Responsive Anti-Counterfeit Nanofingerprints. *Adv. Funct. Mater.* **2016**, *26*, 1315–1321.

Supplementary Information

Color Tuning by Spontaneous Propagation of Gap Surface Plasmons in Epsilon Near Zero Nano-Cavity

Giuseppe Emanuele Lio,[†] Antonio Ferraro,^{*,†} Michele Giocondo,[‡] Roberto
Caputo,^{*,†,¶} and Antonio De Luca[†]

[†]*CNR-Nanotec, Cosenza and Physics Department, University of Calabria,
87036 Arcavacata di Rende (CS), Italy*

[‡]*CNR-Nanotec, Cosenza 87036 Arcavacata di Rende (CS), Italy*

[¶]*Institute of Fundamental and Frontier Sciences, University of Electronic Science and
Technology of China, Chengdu 610054*

E-mail: antonio.ferraro@unical.it; roberto.caputo@unical.it

Abstract

This work presents numerical and experimental results of plasmonic Metal-Insulator-Metal-Insulator nano-cavities with high gain effect. We use Silver as metal and polyvinylpyrrolidone or indium tin oxide or zinc oxide as insulator. The proposed systems exhibit extraordinary effects as colors changing in function of the incident/view angles and a giant enhancement of the experimental real and imaginary parts of the pseudo dielectric constant, a transmission of 50% and zero reflection for both polarizations at the resonant wavelengths. These results confirm the formation of surface plasmon polaritons and their hybridization in gap surface plasmons.

The concurrence of these effects allow the study of the Goos-Hänchen shift by exploiting the very narrow Δ and Ψ parameters. Thank to their optical properties, the proposed nano-cavities could be applied in several fields such tunable color filters, active optics, photonics and sensors.

FigS1a reports experimental and numerical ellipsometer parameters Ψ and Δ for the silver layer ($t = 40nm$), while FigS1b for nano-cavity composed of PVP as insulator.

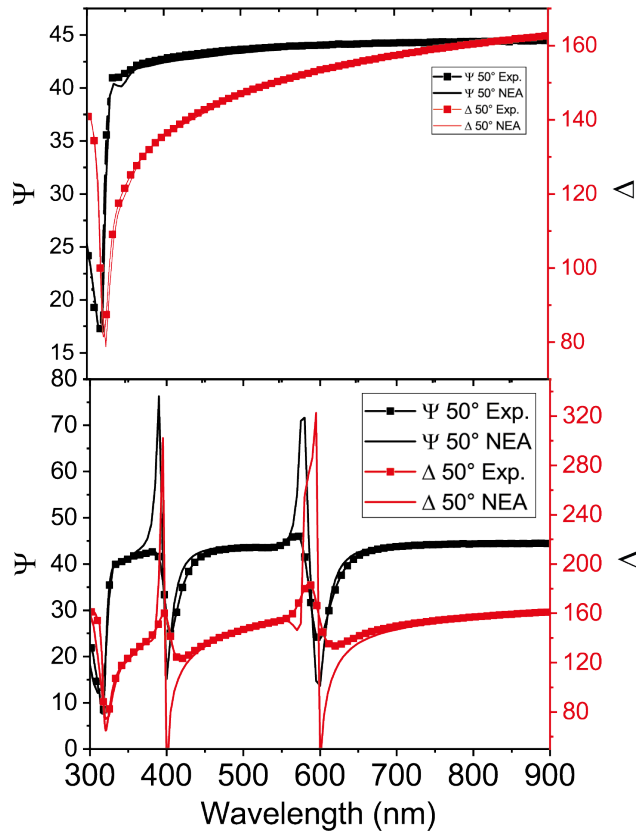


Figure S1: a) Experimental (Exp.) and numerical (NEA) Ψ and Δ of the silver layer ($t = 40nm$). b) Experimental (Exp.) and numerical (NEA) Ψ and Δ of the nano cavity composed of PVP ($t = 380nm$).

The Fig S2a,b shows the numerical comparison between the MIM and MIMI reflectances for the p and s-pol, Ψ and Δ respectively. The presence of a s-polarized reflectance reaching 0% for the MIMI leads to a particular Ψ curve. Indeed, it presents a minimum and maximum corresponding

to the s-pol and p-pol, respectively.

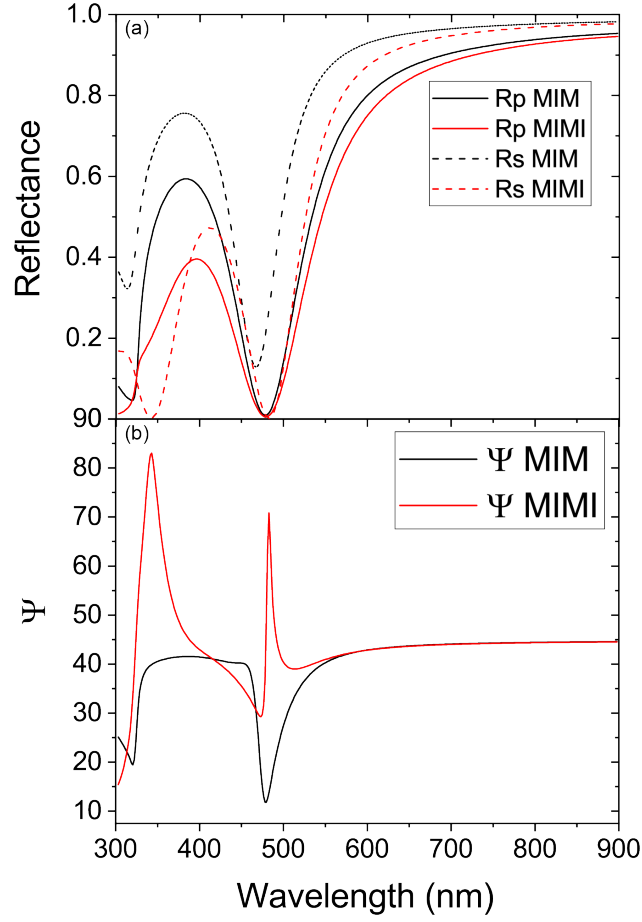


Figure S2: a,b) show the numerical reflectances, Ψ and Δ for the MIM and MIMI.

The Fig S3 shows the experimental reflectance for the s-pol, and the numerical simulations for the reflectances (both polarizations), transmittance and the ellipsometer parameters for the system composed of an ITO layer of $65nm$.

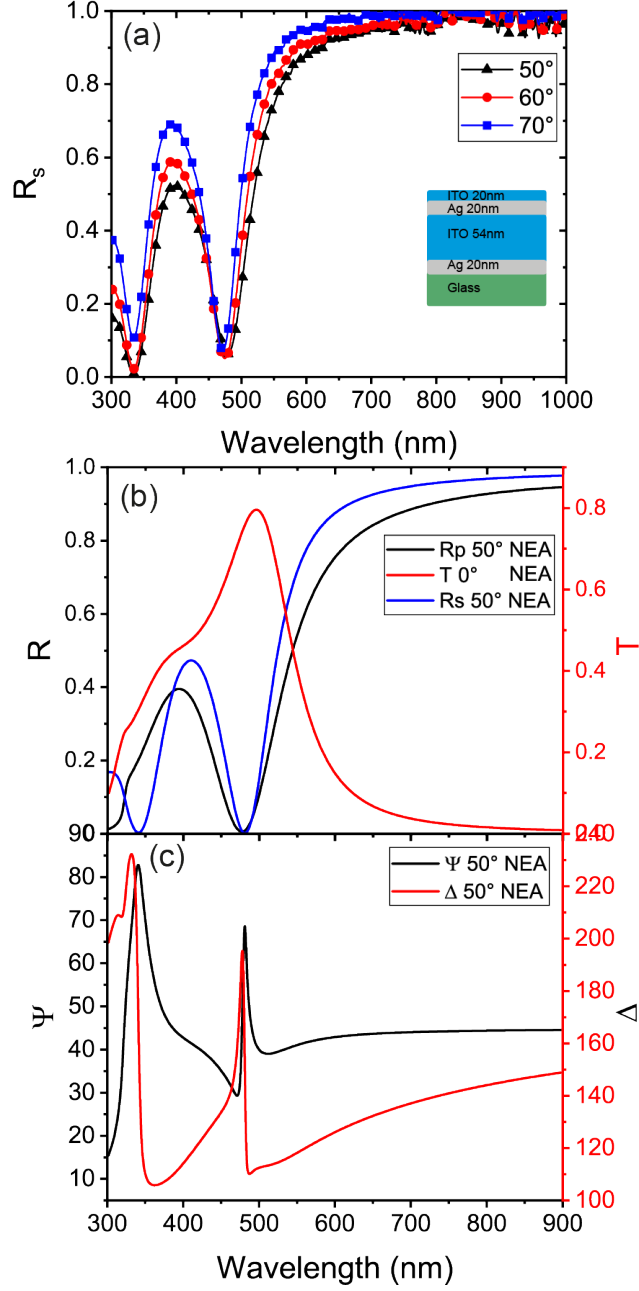


Figure S3: a) Reflectance (s-pol) at different incident angles for the system made by the ITO slab of 65nm. b,c) Numerical results for reflectances (p and s-pol) and transmittance, Ψ and Δ .

Fig S4 shows the experimental reflectance for the s-pol, and the numerical simulations for the reflectances (both polarizations), transmittance and the ellipsometer parameters for the system composed of an ITO layer of 85nm.

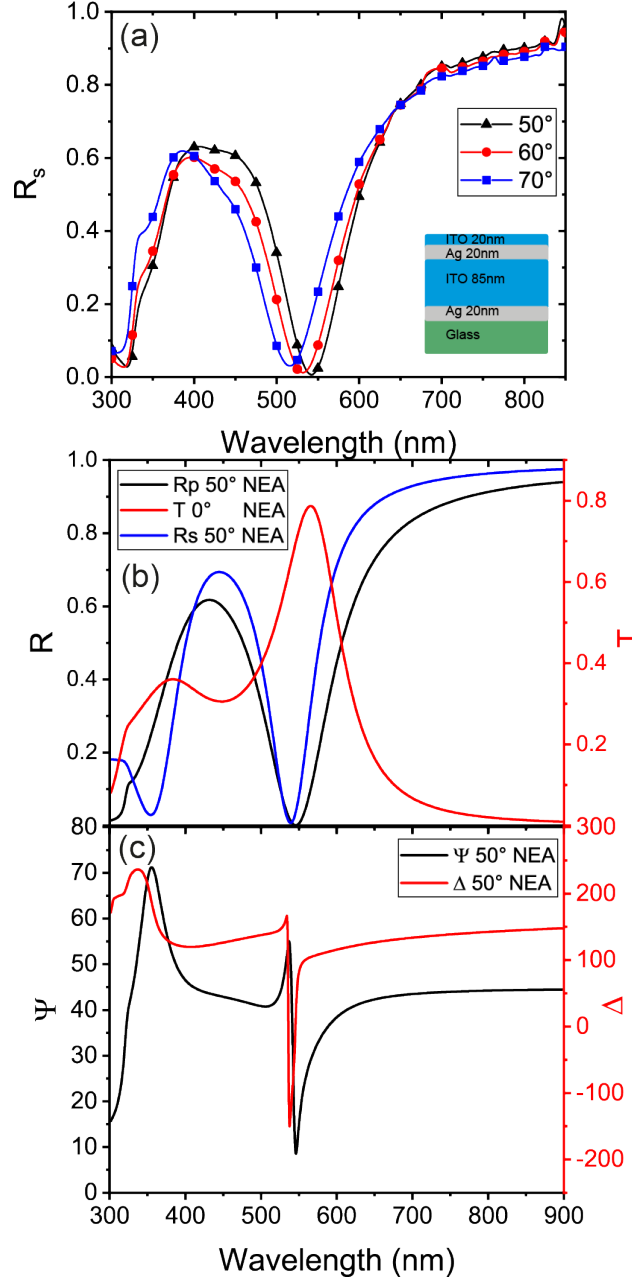


Figure S4: a) Reflectance (s-pol) at different incident angles for the system made by the ITO slab of 85nm. b,c) Numerical results for reflectances (p and s-pol) and transmittance, Ψ and Δ .

Fig S5 shows the electric field maps from an incident electromagnetic wave at 50 degree that impinges on the system composed of a ITO layer of 85nm. We analyzed the system in two main conditions at and out of the resonance.

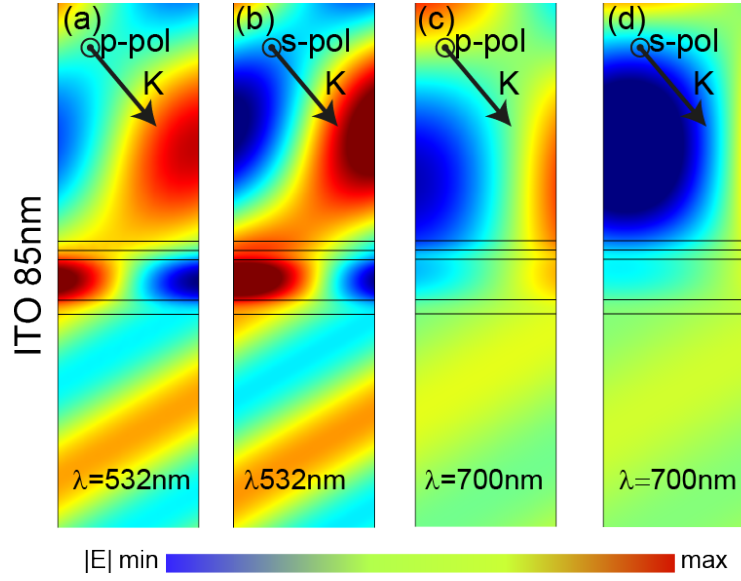


Figure S5: Electric field maps at and out of the resonance for the system composed of an ITO layer of $85nm$. a, b) Electric field maps for p and s-polarization at $\lambda = 532nm$. c, d) The out of resonance for both polarization at $\lambda = 700nm$.

Fig S6 shows the experimental reflectance for the s-pol, and the numerical simulation about the reflectance (both polarizations) transmittance and the ellipsometer parameters for a system composed of a ZnO slab of $83nm$.

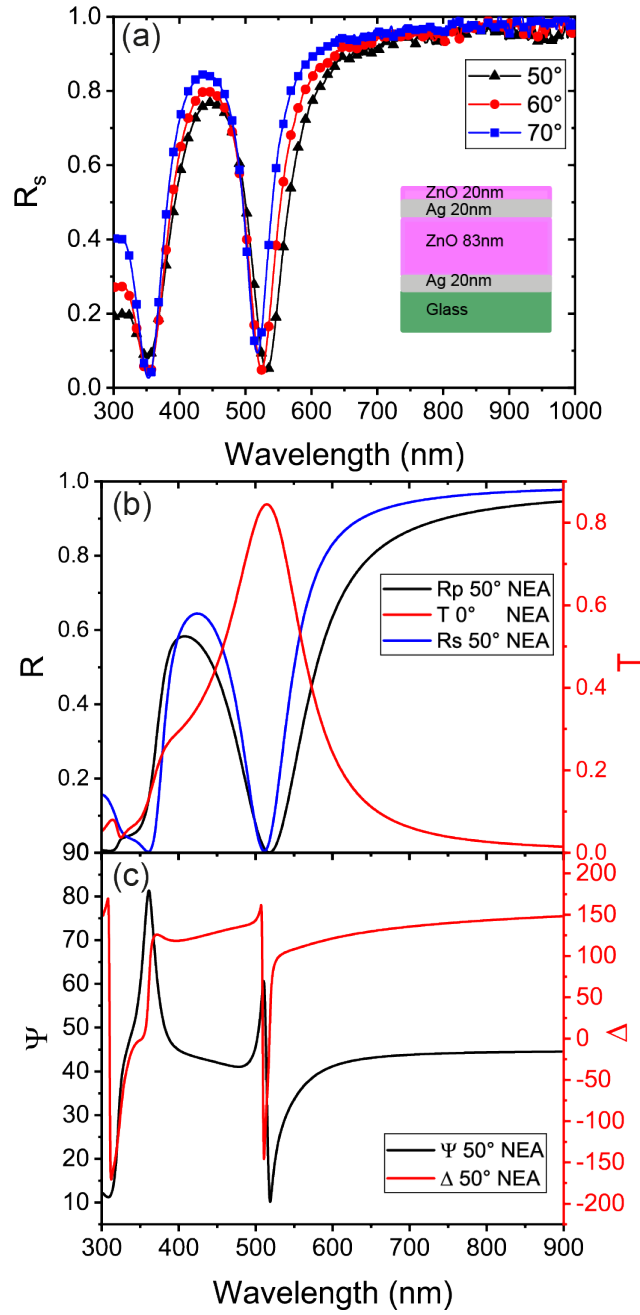


Figure S6: a) Reflectance (s-pol) at different incident angles for the system composed of the ZnO slab of 83nm. b,c) Numerical results for reflectances (p and s-pol) and transmittance, Ψ and Δ .

Fig S7 shows the electric field maps from an incident electromagnetic wave at 50 degree that impinges on the system composed of a ZnO layer of 83nm. We analyzed the system in two main conditions at and out of the resonance.

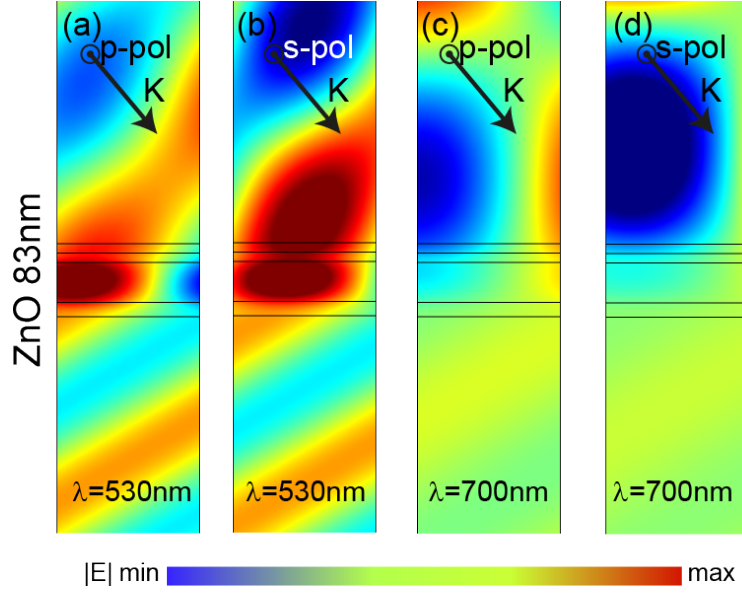


Figure S7: Electric field maps at and out of the resonance for the system composed of a ZnO layer of 83nm. a , b) The electric filed maps for p and s-polarization at $\lambda = 530\text{nm}$. c, d) The out of resonance for both polarization at $\lambda = 700\text{nm}$.

Acknowledgment

The authors thank the “Area della Ricerca di Roma 2”, Tor Vergata, for the access to the ICT Services (ARToV-CNR) for the use of the COMSOL Multiphysics Platform, Origin Lab and Matlab, and the Infrastructure “BeyondNano” (PONa3-00362) of CNR-Nanotec for the access to research instruments.